Autophagy mediates degradation of nuclear lamina

Zhixun Dou[1], Caiyue Xu[1], Greg Donahue[1], Andre Ivanov[2], Ji-An Pan[3], Jiajun Zhu[1], Brian C. Capell[1], Joseph M. Catanzaro[3], M. Daniel Ricketts[4], Takeshi Shimi[7], Trond Lamark[8], Stephen A. Adam[7], Ronen Marmorstein[4, 5, 6], Wei-Xing Zong[3], Robert D. Goldman[7], Terje Johansen[8], Peter D. Adams[2], and Shelley L. Berger[1,9]

[1]Epigenetics Program, Department of Cell and Developmental Biology, Perelman School of Medicine, University of Pennsylvania, Philadelphia, Pennsylvania 19104, USA;

[2]Institute of Cancer Sciences, University of Glasgow, Cancer Research UK Beatson Labs, Glasgow G61 1BD, United Kingdom;

[3]Department of Molecular Genetics and Microbiology, Stony Brook University, Stony Brook, New York 11794, USA;

[4]Department of Biochemistry & Biophysics, [5]Department of Chemistry, [6]Abramson Family Cancer Research Institute, University of Pennsylvania, Philadelphia, Pennsylvania 19104, USA;

[7]Department of Cell and Molecular Biology, Feinberg School of Medicine, Northwestern University, Chicago, Illinois 60611, USA;

[8]Molecular Cancer Research Group, Institute of Medical Biology, University of Tromsø, 9037 Tromsø, Norway.

[9]Correspondence should be addressed to S.L.B. (e-mail:bergers@mail.med.upenn.edu)

Abstract

Autophagy is a catabolic membrane trafficking process involved in degradation of cellular constituents through lysosomes, which maintains cell and tissue homeostasis. While much attention has been focused on autophagic turnover of cytoplasmic materials, little is known regarding the role of autophagy in degrading nuclear components. Here we report that the autophagy machinery mediates degradation of nuclear lamina components in mammalian cells, a process we term laminophagy. The autophagy protein LC3 is present in the nucleus and directly interacts with the nuclear lamina protein Lamin B1, and associates with lamin-associated domains (LADs) on chromatin. This interaction does not downregulate Lamin B1 during starvation, but mediates its degradation upon tumorigenic insults, such as by oncogenic Ras. Laminophagy is achieved by nucleus-to-cytosol transport that delivers Lamin B1 to the lysosome for degradation. Inhibiting autophagy or LC3-Lamin B1 interaction prevents oncogenic Ras-induced Lamin B1 loss and delays oncogene-induced cell cycle arrest. Our study unveils a role for autophagy in degrading nuclear materials, and suggests laminophagy as a guarding mechanism protecting cells from tumorigenesis.

Text

Macroautophagy (hereafter referred to as autophagy) is an evolutionarily conserved trafficking event that forms double-membrane autophagosomes enclosing cellular contents which fuse with late endosomes or lysosomes for degradation of enclosed materials[1-3]. Autophagy maintains cell and tissue integrity, and is essential during starvation[1-4]. Dysfunction of autophagy is involved in a number of diseases[1-3,5-9]. Because autophagosomes are observed in the cytosol, extensive studies have focused on autophagic degradation of cytosolic materials. However, several autophagy proteins have been detected in the nucleus, one of which is the well-known microtubule-associated protein light chain 3 (LC3)[10-13]. LC3 undergoes a ubiquitin-like conjugation modification that couples the lipid phosphatidylethanolamine to LC3 (termed LC3-II) to facilitate its binding to membranes[14-17]. LC3 is involved in autophagosome maturation and delivery of selective autophagy substrates to autophagosomes[16,18,19]. Intriguingly, an abundant pool of LC3 resides in the nucleus in the basal state, and, upon autophagy induction, LC3 diminishes its nuclear abundance and forms cytosolic puncta[10,12,13]. The nuclear mobility of LC3 is slow[13], indicating it may interact with a high molecular-weight complex[13]. However, the nature of this putative interaction is not known.

We initiated this study by investigating LC3 distribution in IMR90 primary human lung fibroblasts, cultured in physiological oxygen (3%). Young proliferating IMR90 cells (population doubling 24) were subjected to subcellular fractionation (Fig. 1a). This revealed a substantial amount of endogenous LC3 in the nuclear fraction, and a small but reproducible amount of lipidated LC3-II in the nucleus (Fig. 1a). Consistent with the presence of nuclear LC3-II, Atg7 and Atg5-Atg12, proteins that mediate LC3 lipidation, are also present in the nucleus in small amounts (Fig. 1a), congruent with recent reports of nuclear functions of Atg5 and Atg7[20,21].

To understand the nuclear binding partners of LC3, we used bacterially purified GST-LC3B (hereafter referred to as LC3, unless specified otherwise) to pull down the isolated nuclear fraction (Fig. 1b). One protein that we found to interact with LC3 is the nuclear lamina protein Lamin B1 (Fig. 1b). The nuclear lamina is a fibrillar network beneath the nuclear envelope, composed of nuclear lamins and associated proteins[22-24]. In addition to providing the nucleus with mechanical strength, nuclear lamina also regulates higher orders of chromatin organization modulating gene expression and silencing[22-24]. In contrast to Lamin B1 binding, Lamins A/C bind poorly to LC3 (Fig. 1b). Using purified Lamin B1 protein (Suppl Fig. 1a), we detected a direct interaction between LC3B and Lamin B1 (Fig. 1c), and found that LC3A and LC3C bind to purified Lamin B1 likewise (Suppl Fig. 1b). Co-immunoprecipitation (co-IP) of endogenous LC3 in HEK293T (Fig. 1d) and IMR90 (Fig. 1e) pulled down endogenous Lamin B1, but little Lamins A/C (Fig. 1d and 1e). In addition, IP of LC3 in IMR90 cytosol and nucleus fractions reveals that the interaction occurs in the nucleus (Fig. 1f). Notably, the Lamin B1-co-precipitated LC3 is

predominately the LC3-II form (Fig. 1e), suggesting LC3 lipidation is involved. Consistent with this, the lipidation deficient LC3-G120A mutant[15] showed impaired binding to Lamin B1 (Fig. 1g); this was specific, as the p62 binding deficient LC3-F52A mutant[25] does not affect the interaction with Lamin B1 (Fig. 1g). Also in contrast to LC3, Beclin 1 and ULK1 showed little or no interaction with Lamin B1 (Fig. 1g). Likewise, Lamin B1 showed decreased binding to LC3 in Atg5-deficient MEFs (Suppl Fig. 1c). Taken together, these data suggest that LC3 directly interacts with Lamin B1, and that LC3 lipidation facilitates this interaction, possibly by tethering LC3 to the nuclear lamina where the interaction occurs. A schematic model is illustrated in Fig. 5f (a).

Lamin B1 is known to associate with transcriptionally inactive heterochromatin domains, termed lamin-associated domains (LADs)[22,23,26]. We used chromatin immunoprecipitation (ChIP) to investigate the association of LC3 with LADs, in proliferating IMR90 cells. ChIP of Lamin B1 coupled with quantitative PCR (qPCR) validated that Lamin B1 associates with LADs but poorly with euchromatin regions, such as β-actin and PCNA promoters (Suppl Fig. 2a). To investigate the interaction of LC3 with chromatin, we first ectopically expressed GFP or GFP-LC3, and performed GFP ChIP. Similarly to Lamin B1 ChIP, GFP-LC3 precipitates LADs but not β-actin or PCNA promoters (Suppl Fig. 2b). This association with LADs is dependent on LC3 lipidation, since the LC3-G120A mutant shows deficient binding to LADs (Fig. 2a, left), although expressed at comparable level to LC3 WT (Fig. 2a, right). We next tested whether endogenous LC3 associates with chromatin. ChIP of endogenous LC3 reveals similar binding to LADs but not the two euchromatic gene promoter regions (Fig. 2b). Knockdown of LC3 by shRNA reduced the signal of LC3 association with LADs (Suppl Fig. 2c), showing the specificity of the LC3 antibody.

We then performed endogenous LC3 ChIP followed by genome-wide parallel sequencing (ChIP-seq) in proliferating IMR90 cells. We mapped LC3 ChIP-seq data to the reference human genome (NCBI v36), quantified binding enrichment by normalization to the number of billions of bases sequenced and to input DNA, and assessed the enrichment map compared to that of our previously published Lamin B1 ChIP-seq[27] (Fig. 2c, example is shown for whole chromosome 10 in upper tracks, and zoom-in view in lower tracks). At the genome-wide scale, LC3 is highly enriched at LADs relative to an equal number of size-matched randomly selected non-LAD control regions (Fig. 2d, Mann-Whitney p-value $<2.2\times10^{-16}$). To further define LC3-associated chromatin, we measured LADs and non-LAD control regions for ChIP-seq enrichment by specific histone markers, including Lys4 trimethylation on histone H3 (H3K4me3) that is canonically associated with active promoters of transcribed genes, and H3K9me3 that represents constitutive heterochromatin regions highly enriched in LADs[28] (Fig. 2e). This analysis revealed that the level of LC3 enrichment strongly correlates with that of Lamin B1 and H3K9me3, but not with H3K4me3, specifically over LADs but not in non-LAD control

regions (Fig. 2e). These data indicate that, at the genome-wide level, LC3 associates with constitutive heterochromatic regions over LADs. Hence, LC3 not only interacts with Lamin B1, but also associates with LADs on chromatin, as illustrated in Fig. 5f (a).

We then probed for possible biological functions of this interaction. Starvation or rapamycin treatment of IMR90 cells caused decreased protein level of autophagy substrate p62 (Fig. 3a), however, Lamin B1 protein level remain unchanged (Fig. 3a). These data indicate that autophagy does not degrade Lamin B1 during starvation. One disruptive scenario that involves Lamin B1 loss is oncogenic insult, such as oncogenic Ras[29-32]. Indeed, most primary cells and tissues cope with oncogenic Ras activity by inducing cellular senescence, a stable cell cycle arrest that serves as a tumor suppressive mechanism[33-35]. We and others have shown that Lamin B1, but not Lamins A/C, is dramatically downregulated during oncogene-induced senescence (OIS), both in vitro and in vivo[29-32]. Importantly, autophagy is upregulated during OIS[36], and autophagic activity has been shown to be required for the mitosis-to-senescence transition[36,37]. Given these connections between autophagy and oncogene activities, we hypothesized that activated oncogenes trigger autophagic degradation of Lamin B1 in primary human cells.

When proliferating IMR90 cells were exposed to oncogenic HRasV12, the cells induce p16INK4a (hereafter referred to as p16), a senescence biomarker, accompanied by downregulation of Lamin B1, but not Lamins A/C (Fig. 3b), consistent with previous findings[31]. Stable expression of GFP-Lamin B1 leads to an expression pattern at the nuclear periphery in proliferating cells (Fig. 3c). Starvation does not alter the Lamin B1 pattern (Fig. 3c). In contrast, HRasV12 expression induces nuclear membrane blebbing, and, occasionally, cytosolic GFP signals (Fig. 3c). Transmission electron microscopy (TEM) analysis of HRasV12-expressing cells confirmed the induction of autophagosomes, reduction of perinuclear heterochromatin, and induction of nuclear membrane blebbing (Suppl Fig. 3a). This nuclear membrane blebbing is morphologically distinct from yeast piecemeal microautophagy[38], in which nuclear blebs are in direct contact with cytosolic vacuoles that result in the pinching-off of nuclear blebs to the vacuoles through nucleus-vacuole junctions[38]. Here we found no evidence of cytosolic vacuoles in direct contact with nuclear blebs (Suppl Fig. 3a).

The weak cytosolic GFP-Lamin B1 signal in HRasV12 cells (Fig. 3c) indicates that it may undergo degradation. In fact, GFP is sensitive to acidic quenching, and by contrast, mCherry is more stable in the acidic environment. Thus a tandem mCherry-GFP fused with an autophagy substrate is useful to track acidic lysosomal degradation[39]. Here, a yellow signal (due to merged mCherry and GFP) indicates the fusion protein is in a normal pH environment, whereas a red signal (due to quenching of GFP) indicates the protein has undergone lysosomal degradation. This technique is frequently used for LC3 and p62 for monitoring autophagy flux[10,12,39]. mCherry-GFP-Lamin B1 showed yellow nuclear peripheral pattern in control cells (Fig. 3d), but displayed cytosolic red signal in

HRasV12-expressing cells (Fig. 3d). Quantitative analysis of the two channels revealed that, while both GFP and mCherry are enriched at the nuclear periphery, mCherry-only fluorescence is detected in the cytosol of HRasV12 cells (Fig. 3d, right panel and graph). These data indicate that Lamin B1 undergoes cytosolic lysosomal degradation. Further, the mCherry-GFP-Lamin B1 technique allowed us to readily quantify that cytosolic Lamin B1 and nuclear membrane blebbing are specifically induced by HRasV12, but not by starvation or rapamycin treatment (Fig. 3e, left and middle groups).

We next performed live-cell imaging with mCherry-GFP-Lamin B1 expressing HRasV12 IMR90 cells (Fig. 3f). This revealed a nucleus-to-cytosol transport process, through nuclear membrane blebbing (as highlighted by arrows in events 1 to 3; see close-up images in lower panels left to right), which then leads to Lamin B1 degradation in the cytosol (note the initial yellow signal, followed by disappearance of GFP then mCherry, in events 1 and 3; event 2 was not yet degraded by the end of the imaging) (Fig. 3f). Because the nuclear export and degradation of Lamin B1 is a dynamic and transient process (Fig. 3f), the results in Fig. 3e are likely underestimated.

The cytosolic Lamin B1 in HRasV12 cells is reminiscent of the cytoplasmic chromatin fragments (CCFs) that we previously described in senescent cells, which are Lamins A/C-negative, but are DAPI-, γ-H2AX- and H3K27me3-positive fragments of heterochromatin budded off from the nuclei, through nuclear membrane blebbing, and are targeted by the lysosomal machinery[31]. Consistent with the behavior of Lamin B1 (Fig. 3e, left and middle groups), we found cytosolic DAPI (that represents the CCFs) specifically appearing in response to HRasV12, but not starvation or rapamycin treatment (Fig. 3e, right group). The cytosolic DAPI staining bodies also stain positive for H3K27me3 (Suppl Fig. 3b and 3c), consistent with our previous observations[31]. Importantly, CCFs colocalize with overexpressed or endogenous LC3 (Suppl Fig. 3b and 3c, and Suppl Fig. 4a and 4b). Moreover, endogenous or overexpressed cytosolic Lamin B1 colocalizes with LC3 (Fig. 3g and Suppl Fig. 3c). In addition, we performed pre-embedded immuno-gold TEM of endogenous Lamin B1. While a gentle detergent in the permeabilization step is beneficial in preserving the ultrastructures, we found that a strong detergent (e.g., Triton X-100) was necessary to deliver the antibody to the nuclear lamina. Although the ultrastructure is compromised, we were able to observe apparent Lamin B1 gold particles beneath the nuclear envelope in control cells (Fig. 3h). In sharp contrast, HRasV12-expressing cells show loss of nuclear lamina signal, and the appearance of cytosolic gold particles, usually in aggregates, inside the autophagic vacuoles (Fig. 3h, and quantified in lower panels). Taken together, these data indicate that Lamin B1 is an autophagy substrate upon oncogene insults, which, through a nucleus-to-cytosol transport process, leads to autophagic degradation in the cytosol, as illustrated in Fig. 5f (b-c).

We subsequently investigated the functional consequence of inhibition of autophagy. Estrogen receptor-tagged HRasV12 was induced by adding 4-hydroxytamoxifen (4-OHT) in IMR90 cells expressing a non-targeting control or an sh-Atg7 hairpin (Fig. 4a). While control cells show progressive downregulation of Lamin B1, Atg7 knockdown cells show reduced LC3 lipidation, and significantly impaired Lamin B1 downregulation (Fig. 4a and quantitation shown in 4b). Lamin B1 mRNA has been shown to decrease upon HRasV12 expression[29,30]. We found that the mRNA level of Lamin B1 is reduced in both control and Atg7 knockdown cells (Suppl Fig. 5a), whereas the protein level of Lamin B1 is maintained in Atg7 deficient cells (Fig. 4a and 4b). These data show that, in response to oncogenic Ras, Lamin B1 is downregulated at both mRNA and protein levels, and that autophagic degradation of the protein is crucial for Lamin B1 loss.

Reduced Lamin B1 is associated with compromised nuclear lamina integrity and barrier function[31,40], resulting in the nuclei being more permeable to fluorescent high molecular weight dextrans[31]. While control HRasV12-expressing cells show nuclear permeation of both 70 and 500-kD dextrans, Atg7 knockdown cells show reduced dextran-positive nuclei (Fig. 4c), indicating increased integrity of the nuclear lamina. In another approach, where we transiently treated primary BJ fibroblasts with the DNA damaging agent etoposide and cultured the cells in regular medium for more than 2 weeks, the cells showed decreased Lamin B1 (Suppl Fig. 5b). In contrast, knockdown of Atg7 (with a different shRNA from used in Fig. 4a) impaired Lamin B1 downregulation (Suppl Fig. 5b). The observation that Lamins A/C remain unchanged (Fig. 3b and Suppl Fig. 5b) is consistent with their inability to interact with LC3 (Fig. 1).

Lamin B1 plays an important role in cell proliferation and senescence[29]. Forced knockdown of Lamin B1 causes impaired proliferation or premature senescence[27,29,40,41]. In line with the compromised degradation of Lamin B1, Atg7 knockdown cells showed delayed HRasV12-induced senescence, as judged by reduced levels of p16 using immunoblotting (Suppl Fig. 5c) and reduced activity of senescence-associated beta-galactosidase (β-gal) (Suppl Fig. 5d), consistent with previous findings that disruption of autophagy delays the onset of oncogene-induced senescence[36,37].

To further dissect the underlying molecular mechanisms, we mapped the LC3-Lamin B1 interaction. Among the critical residues and domains of LC3, LC3 R10 and R11 were found to be essential for binding to Lamin B1, from in vitro pull-down and co-IP experiments (Fig. 4d and Suppl Fig. 6a and 6b). This interaction is unusual compared to other LC3 binding partners[18,19], as the first 28 amino acids of LC3 is sufficient for the interaction, and the LC3 C-terminal ubiquitin-like domain (30-128) is not required for interaction (Fig. 4d).

Due to the redundant roles of LC3 family proteins in binding to Lamin B1 (e.g., Suppl. Fig. 1b), it is difficult to manipulate the interaction in vivo from the LC3 end. We thus

performed an unbiased mapping of Lamin B1 in its interaction with LC3 (Fig. 4e). Using overexpressed or in vitro translated truncations and internal deletions, we found that the linker region between Coil 2 and the Ig-fold of Lamin B1 is necessary for LC3 binding (Fig. 4e, and Suppl Fig. 6c and 6d). Truncation of this region, but not others, resulted in abrogated binding to LC3 in vitro (Fig. 4e, and Suppl Fig. 6c and 6d). Strikingly, this linker region (390-438) is the most evolutionarily conserved domain among all vertebrate Lamin B1 proteins (Fig. 4f), indicating a potentially important function. This region (390-438, 49 amino acids) along with 20 amino-acid flanking sequences at the N- and C-terminus (resulting in an 89 amino-acid fragment 370-458) is sufficient to bind LC3 (Fig. 4e bottom, and Suppl Fig. 7a and 7b), while the 49 amino-acid region itself (390-438) failed to bind LC3 (Fig. 4e and Suppl Fig. 7b), likely due to a defect in proper peptide folding. The 370-458 region of Lamin B1 contains its nuclear localization signal (NLS) (Fig. 4e), and thus the 89 amino-acid fragment localizes to the nucleus (Fig. 4g), and is able to interact with endogenous LC3 (Fig. 4h). We further found that overexpression of this fragment decreases endogenous LC3-Lamin B1 interaction (Fig. 4h), likely due to a competition with Lamin B1 to bind LC3; in contrast, overexpression of the fragment does not affect LC3 lipidation (Fig. 4h), LC3 binding to p62 (Fig. 4h), or p62 degradation upon starvation (Suppl Fig. 7c), indicating an intact autophagy pathway. When expressed in the HRasV12 IMR90 cells, the fragment impaired Lamin B1 downregulation, accompanied by a delayed p16 induction (Fig. 4i), which is a phenocopy of the Atg7 knockdown cells (Fig. 4a and Suppl Fig. 5c). Collectively, these data suggest that inhibiting autophagy or LC3-Lamin B1 interaction causes impaired autophagic degradation of Lamin B1.

We then proceeded to identify the residues in Lamin B1 required for binding to LC3. We first performed 10 amino-acid truncations within the Lamin B1 390-438 region, using in vitro translated proteins, and found that the first 30 amino acids are required for association with LC3 (Suppl. Fig. 8a). This 30 amino-acid region is evolutionarily highly conserved (Suppl. Fig. 8b). Unbiased substitution mutagenesis within this region revealed that residues S393, S395, S396, R397, and V398 are essential for LC3 binding (Fig. 5a and Suppl. Fig. 8c), and simultaneously substituting these residues to alanine abrogated the interaction in vitro (Fig. 5a, hereafter referred to as Lamin B1 Mut), while substituting other residues had little or no effect (Suppl. Fig. 8c). The residues of the NLS of Lamin B1 415-419 are not required for the interaction in vitro (Suppl. Fig. 8c). When expressed in cells, the substitution mutant showed a normal nuclear peripheral pattern (Suppl. Fig. 9a), and is able to interact with endogenous Lamin A and Lamin B1 (Suppl. Fig. 9b), indicating the mutant behaves normally at the nuclear lamina. Co-IP of the Lamin B1 substitution mutant shows deficient binding of endogenous LC3 (Fig. 5b). The remaining slight interaction of the mutant with LC3 (Fig. 5b) is most likely via endogenous Lamin B1 present in cells, as the Lamin B1 substitution mutant shows normal association with endogenous Lamin B1 (Suppl. Fig. 9b) that binds to LC3.

Importantly, when expressed in HRasV12 IMR90 cells, the Lamin B1 mutant showed deficient downregulation compared to WT Lamin B1 (Fig. 5c, compare WT in middle lanes to Mut in right lanes). Further, while mCherry-GFP-Lamin B1 WT HRasV12 cells show cytosolic DAPI (CCF) and cytosolic mCherry signal (Fig. 5d upper panel and Fig. 3d-g), strikingly, the mutant shows dramatically reduced cytosolic DAPI and mCherry signals (Fig. 5d lower panels). In contrast, the mutant displayed massive nuclear membrane blebbings that are unable to export to the cytosol (Fig. 5d). Quantification of more than 200 cells revealed that the mutant has significantly decreased CCF and cytosolic mCherry-Lamin B1, while showing intact ability to induce nuclear membrane blebbing (Fig. 5e). These results indicate that the mutant has a profound deficiency in nucleus-to-cytosol transport. Consequently, the mutant-expressing cells delayed HRasV12-induced senescence with a higher efficiency than WT Lamin B1, as measured by β-gal activity (Suppl. Fig. 9c). In summary, these data strongly suggest that Lamin B1 binding to LC3 is not involved in the step of nuclear membrane blebbing, but is essential for the subsequent nuclear export to cytosol. Blocking the nucleus-to-cytosol transport inhibits laminophagy and delays senescence imposed by oncogenic Ras.

In this study, we presented the first nuclear interaction partner of the autophagy protein LC3, showing that LC3 interacts with Lamin B1 and associated LADs on chromatin (Fig. 5f, a). This interaction specifically mediates laminophagy upon tumorigenic and genotoxic insults, such as by oncogenic Ras and DNA damage (Fig. 5f, b and c). Notably, laminophagy does not occur upon starvation. Recent studies on Lamin B1, including ours, revealed that downregulation of Lamin B1 damages the integrity of the nuclear lamina, reduces cell proliferation or causes premature senescence, and leads to large scale alterations in the epigenome that is associated with global gene expression changes[27,29,31,40,41]. These dramatic changes are beneficial in restraining tumorigenesis, but are unlikely to be the strategies to cope with starvation, a physiological condition that repetitively occurs for all living organisms.

While the detailed molecular mechanisms triggering laminophagy are out of the scope of the current study, our work highlights that autophagy proteins reside at the nuclear lamina in the basal state and trigger laminophagy upon aberrant insults. Inhibiting laminophagy prevents the downregulation of Lamin B1 and delays oncogene-induced cell cycle arrest, as shown, first, by Atg7 knockdown, second, by overexpression of Lamin B1 peptide that competes endogenous LC3-Lamin B1 binding, and, third, by expression of a Lamin B1 substitution mutant that fails to associate with LC3. Thus, laminophagy serves as a potential guarding mechanism, protecting cells and tissues from oncogenic transformation. In addition to oncogene activation, laminophagy may function in other scenarios. Recent studies show that autophagy contributes to degradation of mutant lamin proteins in laminopathies[42,43], a group of genetic diseases caused by mutations of nuclear lamin proteins[24,44,45]. Additionally, stress associated with cancer cells produces

micronuclei and/or cytosolic chromatin, which can mediate cancer cell death[46,47]. Finally, we have previously detected cytosolic chromatins in aged tissue[31]. Taken together, these studies suggest that laminophagy responds to abnormal cellular insults, and may play a role in maintaining cell and tissue integrity. Dysregulated laminophagy may therefore contribute to tumorigenesis and age-related diseases.

While our current work focused on LC3 and Lamin B1, we anticipate that other autophagy proteins/interactions have roles in the nucleus in orchestrating laminophagy and other physiological conditions. This study establishes a new angle in understanding autophagy from the perspective of the nucleus.

Methods

Complete methods are described in supplemental information.

Acknowledgements

We thank members of the Berger lab and Adams lab for technical assistance and discussions. We acknowledge Dr. Andrea L. Stout for the help on confocal microscopy, and the electron microscopy resource laboratory for the assistance on TEM. We thank Drs. Barry Zee and Benjamin Garcia for the work of mass-spectrometry, and Dr. Zhenyu Yue for critical reading of the manuscript. Dr. Zhixun Dou is supported by the fellow award from The Leukemia & Lymphoma Society. Dr. Brian C. Capell is supported by career development awards from the Dermatology Foundation, Melanoma Research Foundation, and American Skin Association. Work from the Berger, Adams, and Marmorstein laboratories are supported by NIA P01 grant (P01AG031862). The Goldman laboratory is supported by R01 GM106023, R01 CA031760 and the Progeria Research Foundation.

References

1 Mizushima, N., Levine, B., Cuervo, A. M. & Klionsky, D. J. Autophagy fights disease through cellular self-digestion. *Nature* **451**, 1069-1075, doi:10.1038/nature06639 (2008).

2 Levine, B. & Kroemer, G. Autophagy in the pathogenesis of disease. *Cell* **132**, 27-42, doi:10.1016/j.cell.2007.12.018 (2008).

3 Rabinowitz, J. D. & White, E. Autophagy and metabolism. *Science* **330**, 1344-1348, doi:10.1126/science.1193497 (2010).

4 Kuma, A. *et al.* The role of autophagy during the early neonatal starvation period. *Nature* **432**, 1032-1036, doi:10.1038/nature03029 (2004).
5 Mathew, R., Karantza-Wadsworth, V. & White, E. Role of autophagy in cancer. *Nature reviews. Cancer* **7**, 961-967, doi:10.1038/nrc2254 (2007).
6 Levine, B., Mizushima, N. & Virgin, H. W. Autophagy in immunity and inflammation. *Nature* **469**, 323-335, doi:10.1038/nature09782 (2011).
7 Choi, A. M., Ryter, S. W. & Levine, B. Autophagy in human health and disease. *The New England journal of medicine* **368**, 1845-1846, doi:10.1056/NEJMc1303158 (2013).
8 Komatsu, M. *et al.* Loss of autophagy in the central nervous system causes neurodegeneration in mice. *Nature* **441**, 880-884, doi:10.1038/nature04723 (2006).
9 Nixon, R. A. The role of autophagy in neurodegenerative disease. *Nature medicine* **19**, 983-997, doi:10.1038/nm.3232 (2013).
10 Klionsky, D. J. *et al.* Guidelines for the use and interpretation of assays for monitoring autophagy in higher eukaryotes. *Autophagy* **4**, 151-175 (2008).
11 Mizushima, N., Yamamoto, A., Matsui, M., Yoshimori, T. & Ohsumi, Y. In vivo analysis of autophagy in response to nutrient starvation using transgenic mice expressing a fluorescent autophagosome marker. *Molecular biology of the cell* **15**, 1101-1111, doi:10.1091/mbc.E03-09-0704 (2004).
12 Mizushima, N., Yoshimori, T. & Levine, B. Methods in mammalian autophagy research. *Cell* **140**, 313-326, doi:10.1016/j.cell.2010.01.028 (2010).
13 Drake, K. R., Kang, M. & Kenworthy, A. K. Nucleocytoplasmic distribution and dynamics of the autophagosome marker EGFP-LC3. *PloS one* **5**, e9806, doi:10.1371/journal.pone.0009806 (2010).
14 Kabeya, Y. *et al.* LC3, a mammalian homologue of yeast Apg8p, is localized in autophagosome membranes after processing. *The EMBO journal* **19**, 5720-5728, doi:10.1093/emboj/19.21.5720 (2000).
15 Kabeya, Y. *et al.* LC3, GABARAP and GATE16 localize to autophagosomal membrane depending on form-II formation. *Journal of cell science* **117**, 2805-2812, doi:10.1242/jcs.01131 (2004).
16 Mizushima, N., Yoshimori, T. & Ohsumi, Y. The role of Atg proteins in autophagosome formation. *Annual review of cell and developmental biology* **27**, 107-132, doi:10.1146/annurev-cellbio-092910-154005 (2011).
17 Mizushima, N. *et al.* A protein conjugation system essential for autophagy. *Nature* **395**, 395-398, doi:10.1038/26506 (1998).
18 Rogov, V., Dotsch, V., Johansen, T. & Kirkin, V. Interactions between autophagy receptors and ubiquitin-like proteins form the molecular basis for selective autophagy. *Mol Cell* **53**, 167-178, doi:10.1016/j.molcel.2013.12.014 (2014).
19 Birgisdottir, A. B., Lamark, T. & Johansen, T. The LIR motif - crucial for selective autophagy. *Journal of cell science* **126**, 3237-3247, doi:10.1242/jcs.126128 (2013).
20 Lee, I. H. *et al.* Atg7 modulates p53 activity to regulate cell cycle and survival during metabolic stress. *Science* **336**, 225-228, doi:10.1126/science.1218395 (2012).

21 Simon, H. U., Yousefi, S., Schmid, I. & Friis, R. ATG5 can regulate p53 expression and activation. *Cell death & disease* **5**, e1339, doi:10.1038/cddis.2014.308 (2014).
22 Dechat, T. *et al.* Nuclear lamins: major factors in the structural organization and function of the nucleus and chromatin. *Genes & development* **22**, 832-853, doi:10.1101/gad.1652708 (2008).
23 Shimi, T. *et al.* The A- and B-type nuclear lamin networks: microdomains involved in chromatin organization and transcription. *Genes & development* **22**, 3409-3421, doi:10.1101/gad.1735208 (2008).
24 Young, S. G., Jung, H. J., Lee, J. M. & Fong, L. G. Nuclear lamins and neurobiology. *Mol Cell Biol* **34**, 2776-2785, doi:10.1128/MCB.00486-14 (2014).
25 Shvets, E., Fass, E., Scherz-Shouval, R. & Elazar, Z. The N-terminus and Phe52 residue of LC3 recruit p62/SQSTM1 into autophagosomes. *Journal of cell science* **121**, 2685-2695, doi:10.1242/jcs.026005 (2008).
26 Guelen, L. *et al.* Domain organization of human chromosomes revealed by mapping of nuclear lamina interactions. *Nature* **453**, 948-951, doi:10.1038/nature06947 (2008).
27 Shah, P. P. *et al.* Lamin B1 depletion in senescent cells triggers large-scale changes in gene expression and the chromatin landscape. *Genes & development* **27**, 1787-1799, doi:10.1101/gad.223834.113 (2013).
28 Barski, A. *et al.* High-resolution profiling of histone methylations in the human genome. *Cell* **129**, 823-837, doi:10.1016/j.cell.2007.05.009 (2007).
29 Shimi, T. *et al.* The role of nuclear lamin B1 in cell proliferation and senescence. *Genes & development* **25**, 2579-2593, doi:10.1101/gad.179515.111 (2011).
30 Freund, A., Laberge, R. M., Demaria, M. & Campisi, J. Lamin B1 loss is a senescence-associated biomarker. *Molecular biology of the cell* **23**, 2066-2075, doi:10.1091/mbc.E11-10-0884 (2012).
31 Ivanov, A. *et al.* Lysosome-mediated processing of chromatin in senescence. *J Cell Biol* **202**, 129-143, doi:10.1083/jcb.201212110 (2013).
32 Sadaie, M. *et al.* Redistribution of the Lamin B1 genomic binding profile affects rearrangement of heterochromatic domains and SAHF formation during senescence. *Genes & development* **27**, 1800-1808, doi:10.1101/gad.217281.113 (2013).
33 Serrano, M., Lin, A. W., McCurrach, M. E., Beach, D. & Lowe, S. W. Oncogenic ras provokes premature cell senescence associated with accumulation of p53 and p16INK4a. *Cell* **88**, 593-602 (1997).
34 Collado, M., Blasco, M. A. & Serrano, M. Cellular senescence in cancer and aging. *Cell* **130**, 223-233, doi:10.1016/j.cell.2007.07.003 (2007).
35 Collado, M. & Serrano, M. Senescence in tumours: evidence from mice and humans. *Nature reviews. Cancer* **10**, 51-57, doi:10.1038/nrc2772 (2010).
36 Young, A. R. *et al.* Autophagy mediates the mitotic senescence transition. *Genes & development* **23**, 798-803, doi:10.1101/gad.519709 (2009).
37 Liu, H. *et al.* Down-regulation of autophagy-related protein 5 (ATG5) contributes to the pathogenesis of early-stage cutaneous melanoma. *Science translational medicine* **5**, 202ra123, doi:10.1126/scitranslmed.3005864 (2013).

38 Roberts, P. *et al.* Piecemeal microautophagy of nucleus in Saccharomyces cerevisiae. *Molecular biology of the cell* **14**, 129-141, doi:10.1091/mbc.E02-08-0483 (2003).
39 Pankiv, S. *et al.* p62/SQSTM1 binds directly to Atg8/LC3 to facilitate degradation of ubiquitinated protein aggregates by autophagy. *J Biol Chem* **282**, 24131-24145, doi:10.1074/jbc.M702824200 (2007).
40 Vergnes, L., Peterfy, M., Bergo, M. O., Young, S. G. & Reue, K. Lamin B1 is required for mouse development and nuclear integrity. *Proceedings of the National Academy of Sciences of the United States of America* **101**, 10428-10433, doi:10.1073/pnas.0401424101 (2004).
41 Dreesen, O. *et al.* Lamin B1 fluctuations have differential effects on cellular proliferation and senescence. *J Cell Biol* **200**, 605-617, doi:10.1083/jcb.201206121 (2013).
42 Park, Y. E. *et al.* Autophagic degradation of nuclear components in mammalian cells. *Autophagy* **5**, 795-804 (2009).
43 Cao, K. *et al.* Rapamycin reverses cellular phenotypes and enhances mutant protein clearance in Hutchinson-Gilford progeria syndrome cells. *Science translational medicine* **3**, 89ra58, doi:10.1126/scitranslmed.3002346 (2011).
44 Capell, B. C. & Collins, F. S. Human laminopathies: nuclei gone genetically awry. *Nature reviews. Genetics* **7**, 940-952, doi:10.1038/nrg1906 (2006).
45 Worman, H. J., Fong, L. G., Muchir, A. & Young, S. G. Laminopathies and the long strange trip from basic cell biology to therapy. *The Journal of clinical investigation* **119**, 1825-1836, doi:10.1172/JCI37679 (2009).
46 Changou, C. A. *et al.* Arginine starvation-associated atypical cellular death involves mitochondrial dysfunction, nuclear DNA leakage, and chromatin autophagy. *Proceedings of the National Academy of Sciences of the United States of America* **111**, 14147-14152, doi:10.1073/pnas.1404171111 (2014).
47 Rello-Varona, S. *et al.* Autophagic removal of micronuclei. *Cell Cycle* **11**, 170-176, doi:10.4161/cc.11.1.18564 (2012).

Figure Legends

Figure 1. LC3 interacts with nuclear lamina protein Lamin B1.
a, Proliferating young IMR90 (PD24) cultured in 3% oxygen was subjected to subcellular fractionation and probed for indicated antibodies. **b**, The nucleus fraction of IMR90 as in **a** was pulled down with bacterially expressed and purified GST or GST-LC3B, and probed with Lamin antibodies. Quantification of relative binding to LC3 is shown on right. Data shown are the average values of three independent experiments. Error bars: s.e.m. * $p<0.0001$. **c**, GST-LC3B pulldown of purified Lamin B1 protein, showing a direct interaction. **d** and **e**, Endogenous co-IP in HEK293T (**d**) and IMR90 (**e**). **f**, The cytosol and nucleus fractions of IMR90 were subjected to LC3 IP. The IP and input are shown. **g**, HEK293T cells were transfected with GFP-tagged constructs, and subjected to GFP IP and western blot analysis. Relative binding of Lamin B1 is quantified and shown on right. Data are the mean values of three independent experiments. Error bars: s.e.m. * $p<0.001$.

Figure 2. LC3 associates with LADs on chromatin.
a, IMR90 (PD24) stably expressing GFP-tagged constructs were subjected to ChIP with GFP antibody, and qPCR for LADs primers or promoter regions of β-actin and PCNA. Results shown are the average values of three independent experiments. Error bars: s.e.m. * $p<0.05$, ** $p<0.01$, mutant compared with WT, n.s., non-significant. Immunoblots of the input and GFP IP are shown on right. **b**, LC3 ChIP of young proliferating IMR90 cells, and qPCR quantitation of LADs and two promoter regions. Results shown are the mean values of three independent experiments. Error bars: s.e.m. * $p<0.01$, ** $p<0.005$, n.s., non-significant. **c-e,** ChIP-seq analysis of LC3 in proliferating IMR90 cells (PD24), revealing colocalization of LC3 and Lamin B1. **c**, Upper: Representative tracks of LC3 and previously published Lamin B1 and LADs over chromosome 10. LC3 is shown in blue, and Lamin B1 and LADs are shown in yellow. Lower: Representative zoom-in view over a 500 kb region on chromosome 10 (chr10: 99,449,723-99,949,723), showing a LAD. Note the apparent overlap of LC3 over LADs. The relative position of this region is indicated with a black line under the upper track. **d**, Box plot representation of Lamin B1 and LC3 ChIP-seq enrichment aligned to LADs and randomly selected non-LAD control regions, showing a preferential enrichment of LC3 in LADs (data presented are the ratio of ChIP-seq tags to input, log2 scale; Mann-Whitney test, *** $p<2.2\times10^{-16}$). **e**, Correlation heat plot of LC3 and Lamin B1 with H3K4me3 and H3K9me3 ChIP-seq, over randomly selected non-LAD control regions or LADs, revealing that LC3, Lamin B1, and H3K9me3 correlate strongly in LADs but not in control regions. Data shown are normalized against corresponding background for each ChIP.

Figure 3. Lamin B1 is an autophagy substrate in response to oncogene insult.
a, IMR90 cells were left untreated or treated with amino-acid starvation, amino-acid plus serum starvation, or rapamycin (500 nM) for 1 and 2 days. Cell lysates were subjected to immunoblotting. **b**, IMR90 cells were infected with control virus or retrovirus expressing HRasV12 for 7 days, and subjected to immunoblotting analysis. **c**, IMR90 stably expressing GFP-Lamin B1 were left untreated or starved in Hanks buffer for 1 day or infected with HRasV12 for 7 days. Representative confocal fluorescent microscopy images are shown. Note the nuclear membrane blebbing and cytosolic GFP, as indicated

by arrows. **d**, IMR90 stably expressing mCherry-GFP-Lamin B1 were infected with control virus or HRasV12 virus for 7 days. Representative confocal microscopy images are shown. Quantification of fluorescent intensities of mCherry and GFP channels are shown on right. **e**, mCherry-GFP-Lamin B1 IMR90 were treated with indicated, and quantification of each condition is shown. Data presented are the mean values of 4 different fields with over 200 cells. Error bars: s.d. * $p<0.01$, ** $p<0.001$. **f**, mCherry-GFP-Lamin B1 HRasV12 IMR90 were imaged for a duration of overnight under spinning-disc confocal microscopy. Images were taken every 15 mins, and representative pictures are shown from one cell. Image shown are the maximum-projection combining all Z-sections. Nucleus-to-cytosol transport events are labelled sequentially as indicated. Selected events are highlighted in insets. Note the nuclear export of events 1-3, and disappearance of events 1 and 3. Event 2 was not yet degraded by the end of the imaging. **g**, mCherry-GFP-Lamin B1 IMR90 cells were stained with LC3 antibody, and imaged under confocal microscopy. Representative images are shown. CCFs are denoted by arrows. **h**, Control and HRasV12 IMR90 cells were subjected to pre-embedded staining with Lamin B1 antibody and were gold-enhanced. Sections were processed for TEM analysis. Representative nuclear lamina in control cells and autophagic vacuoles are shown in insets. Quantification with over 20 randomly selected and imaged cells are shown at the bottom. Error bars: s.e.m.

Figure 4. Inhibiting autophagy or LC3-Lamin B1 interaction impairs Lamin B1 degradation.

a, ER:HRasV12 IMR90 cells were stably infected with lentivirus encoding non-targeting control hairpin (sh-NTC) or sh-Atg7 hairpin. HRasV12 was induced by addition of 4-OHT for indicated days. Cell lysates were analyzed by western blotting with antibodies indicated. **b**, Quantification of Lamin B1 from western blotting of three independent experiments. Error bars: s.e.m. * $p<0.05$, ** $p<0.005$, *** $p<0.0001$, compared with sh-NTC Day 0. n.s., non-significant. **c**, Nuclei from indicated cells were incubated with 70 kDa or 500 kDa Dextrans, and Dextran positive nuclei were scored. Results shown are the average values of three independent scorings. Error bars: s.d. * $p<0.005$. **d**, Purified Lamin B1 protein was subjected to GST pull-down of GST-LC3B WT or mutants. Note that the R10A/R11A mutant shows impaired binding to Lamin B1. **e**, Schematic illustration of Lamin B1 mutants in binding to LC3. **f**, Conservation analysis of Lamin B1 domains in vertebrates. Within each domain, the number of conserved residues is calculated and normalized to the total number of residues. All residues in Lamin B1 are quantified and presented as total. **g,** mCherry-GFP-Lamin B1 370-458 was stably expressed in IMR90 and imaged under confocal microscopy. **h**, HEK293T transfected with mCherry-GFP tagged proteins were subjected to LC3 IP, and analyzed as indicated. **i**, ER:HRasV12 IMR90 cells stably expressing indicated constructs were harvested every two days, and subjected to western blotting analysis.

Figure 5. Lamin B1 mutant that does not bind to LC3 shows deficiency in nucleus-to-cytosol transport.

a, In vitro translated Lamin B1 mutants were subjected to GST-LC3 pulldown. The pulldown and input are shown. Results shown are representative of three independent experiments. **b**, HEK293T cells were transfected with Lamin B1 WT or mutant construct,

and subjected to LC3 IP and immunoblotting analysis. **c**, ER:HRasV12 IMR90 cells expressing WT or mutant Lamin B1 were induced with 4-OHT and harvested at indicated days. Cell lysates were analyzed with indicated antibodies. **d**, mCherry-GFP-Lamin B1 WT or Mut expressing HRasV12 IMR90 cells were analyzed under confocal microscopy. Cells were harvested at Day 6 post Ras induction. Note that while WT Lamin B1 cells show cytosolic DAPI and mCherry, the Mut cells show massive nuclear membrane blebbings, but are deficient in nuclear export to cytosol. **e**, Cells as in **d** were quantified for cytosolic DAPI (CCF), cytosolic mCherry signal (cytosolic Lamin B1), and nuclear membrane blebbing. Results presented are the mean values from no less than 4 different fields with over 200 cells. Error bars: s.d. * $p<0.05$, ** $p<0.005$, *** $p<0.0001$. **f**, Schematic illustration of laminophagy. **(a),** In the basal state, nuclear LC3 resides at nuclear lamina through its lipidation. The un-lipidated LC3 is localized in nuclear plasma that does not associate with nuclear lamina. Note that LC3 also associates with LADs on chromatin. **(b and c)**, Upon nuclear lamina damage (e.g. by oncogene), nuclear membrane blebbing is formed that transports pieces of nuclear lamina to cytosol, forming the cytoplasmic chromatin fragments (CCFs) that are initially positive for DAPI, Lamin B1, and LC3. The CCFs are then targeted by cytosolic autophagy machinery, leading to autophagic degradation.

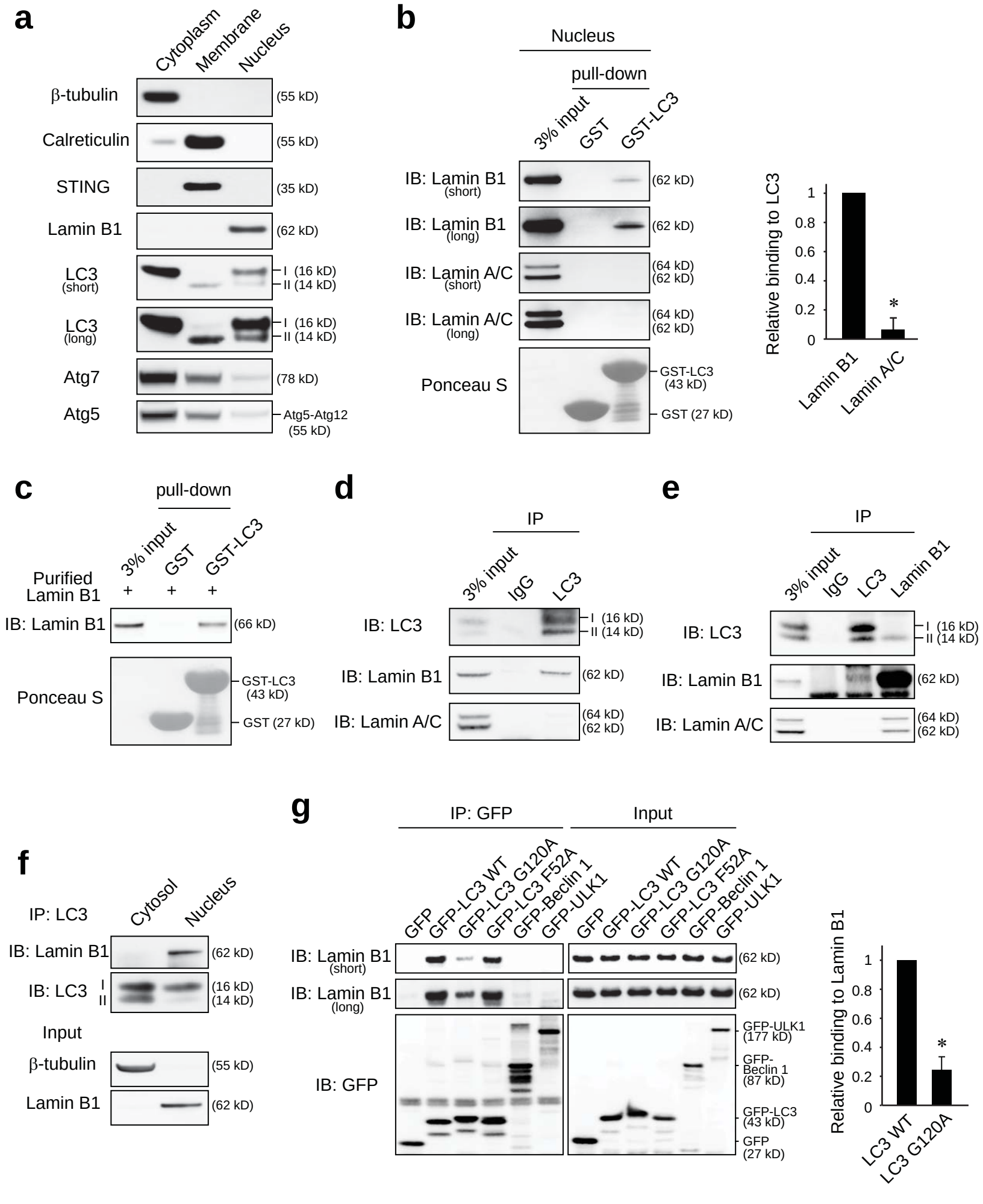
a
Cytoplasm
Membrane
Nucleus
β-tubulin
(55 kD)
Calreticulin
(55 kD)
STING
(35 kD)
Lamin B1
(62 kD)
LC3 (short)
I (16 kD)
II (14 kD)
LC3 (long)
I (16 kD)
II (14 kD)
Atg7
(78 kD)
Atg5
Atg5-Atg12 (55 kD)
b
Nucleus
pull-down
3% input
GST
GST-LC3
IB: Lamin B1 (short)
(62 kD)
IB: Lamin B1 (long)
(62 kD)
IB: Lamin A/C (short)
(64 kD) (62 kD)
IB: Lamin A/C (long)
(64 kD) (62 kD)
Ponceau S
GST-LC3 (43 kD)
GST (27 kD)
Relative binding to LC3
1
0.8
0.6
0.4
0.2
0
*
Lamin B1
Lamin A/C
c
pull-down
3% input
GST
GST-LC3
Purified Lamin B1
+ + +
IB: Lamin B1
(66 kD)
Ponceau S
GST-LC3 (43 kD)
GST (27 kD)
d
IP
3% input
IgG
LC3
IB: LC3
I (16 kD)
II (14 kD)
IB: Lamin B1
(62 kD)
IB: Lamin A/C
(64 kD) (62 kD)
e
IP
3% input
IgG
LC3
Lamin B1
IB: LC3
I (16 kD)
II (14 kD)
IB: Lamin B1
(62 kD)
IB: Lamin A/C
(64 kD) (62 kD)
f
IP: LC3
Cytosol
Nucleus
IB: Lamin B1
(62 kD)
IB: LC3
I
II
(16 kD) (14 kD)
Input
β-tubulin
(55 kD)
Lamin B1
(62 kD)
g
IP: GFP
Input
GFP
GFP-LC3 WT
GFP-LC3 G120A
GFP-LC3 F52A
GFP-Beclin 1
GFP-ULK1
IB: Lamin B1 (short)
(62 kD)
IB: Lamin B1 (long)
(62 kD)
IB: GFP
GFP-ULK1 (177 kD)
GFP-Beclin 1 (87 kD)
GFP-LC3 (43 kD)
GFP (27 kD)
Relative binding to Lamin B1
1
0.8
0.6
0.4
0.2
0
*
LC3 WT
LC3 G120A

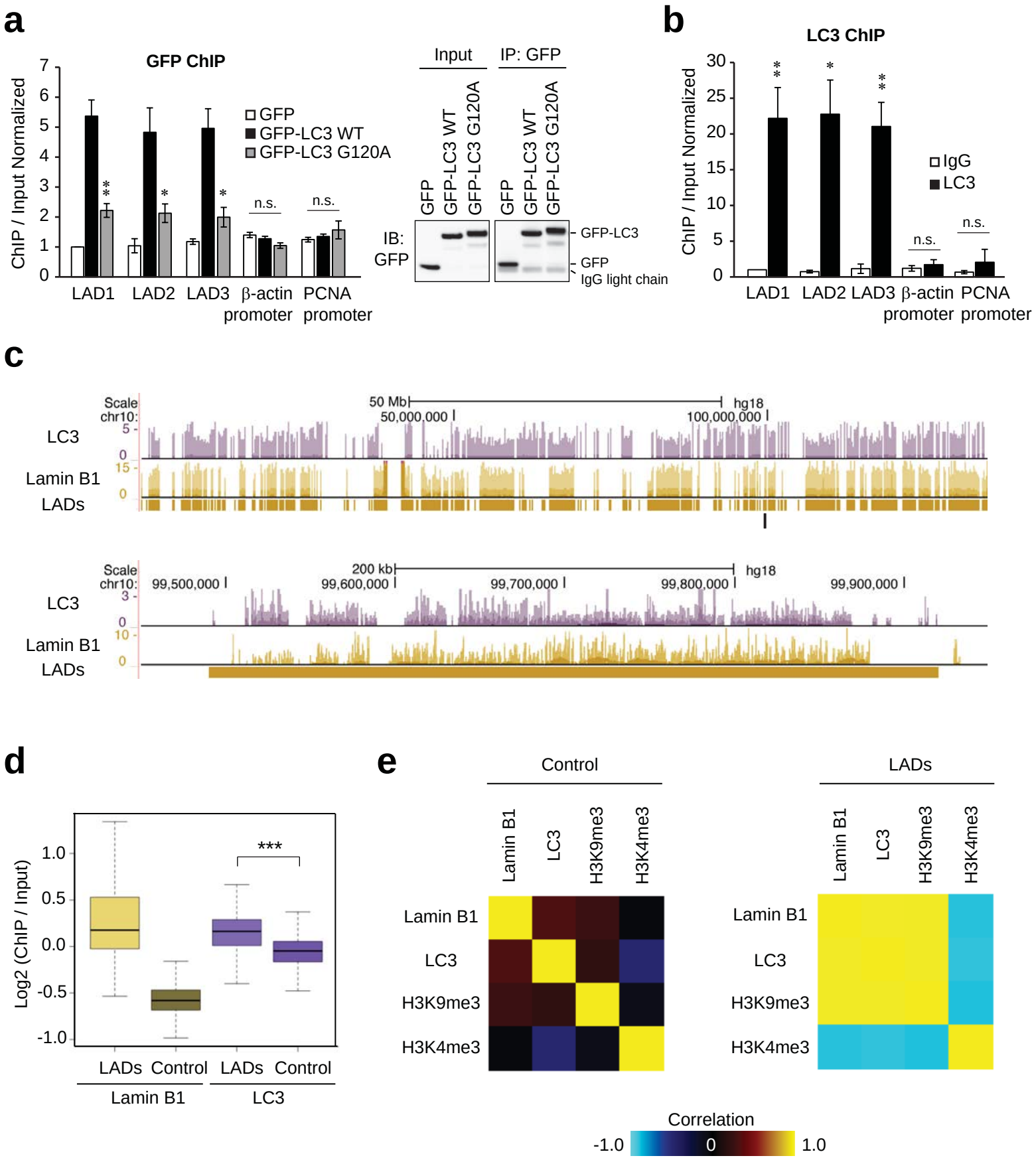
a
GFP ChIP
ChIP / Input Normalized
GFP
GFP-LC3 WT
GFP-LC3 G120A
LAD1
LAD2
LAD3
β-actin promoter
PCNA promoter
n.s.
Input
IP: GFP
IB: GFP
GFP-LC3
GFP
IgG light chain
b
LC3 ChIP
ChIP / Input Normalized
IgG
LC3
c
Scale
chr10:
50 Mb
50,000,000
100,000,000
hg18
LC3
Lamin B1
LADs
200 kb
99,500,000
99,600,000
99,700,000
99,800,000
99,900,000
d
Log2 (ChIP / Input)
***
LADs
Control
Lamin B1
LC3
e
Control
LADs
Lamin B1
LC3
H3K9me3
H3K4me3
Correlation
-1.0
0
1.0

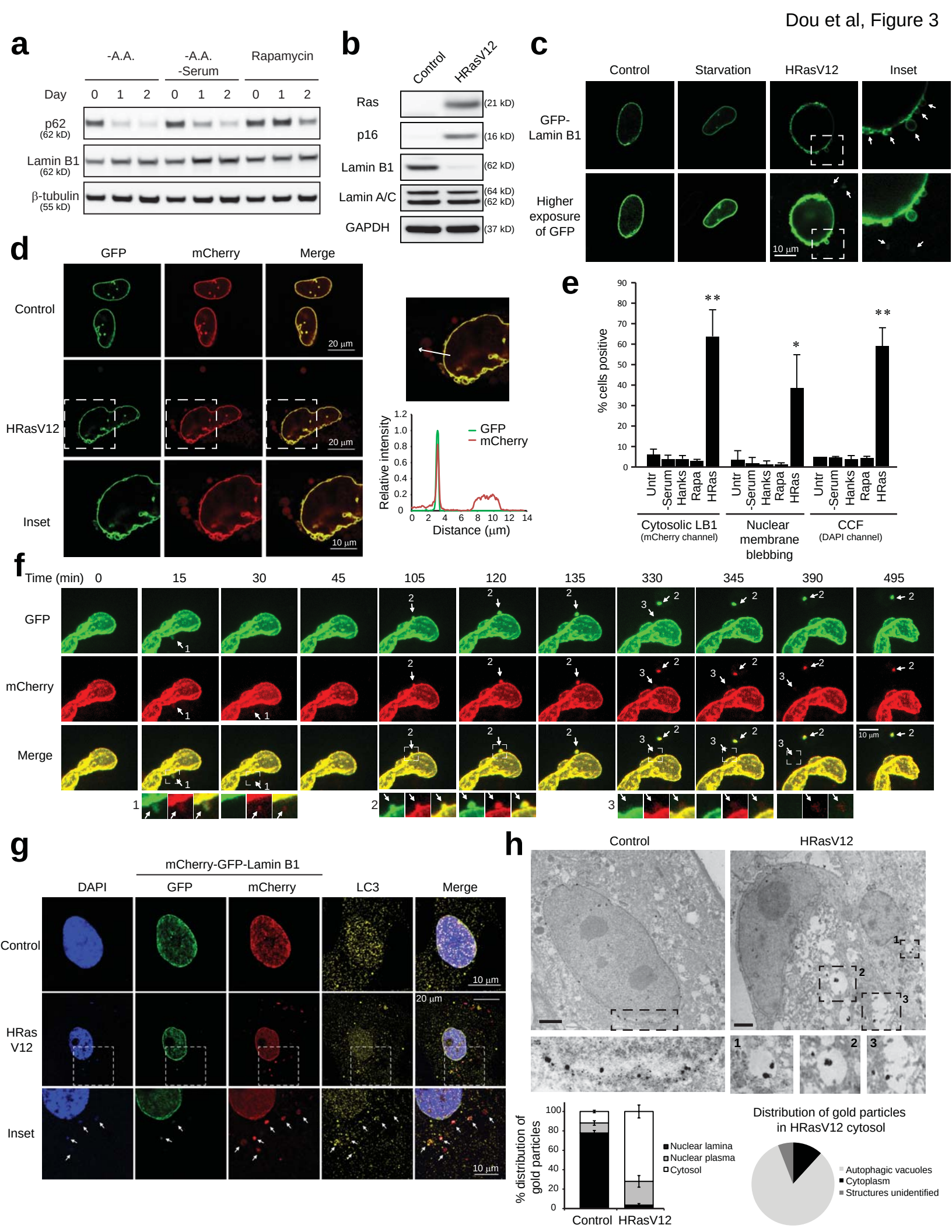
a
-A.A.
-A.A. -Serum
Rapamycin
Day 0 1 2 0 1 2 0 1 2
p62 (62 kD)
Lamin B1 (62 kD)
β-tubulin (55 kD)
b
Control
HRasV12
Ras (21 kD)
p16 (16 kD)
Lamin B1 (62 kD)
Lamin A/C (64 kD) (62 kD)
GAPDH (37 kD)
c
Control
Starvation
HRasV12
Inset
GFP-Lamin B1
Higher exposure of GFP
10 μm
d
GFP
mCherry
Merge
Control
HRasV12
Inset
20 μm
10 μm
Relative intensity
Distance (μm)
GFP
mCherry
e
% cells positive
Untr
-Serum
Hanks
Rapa
HRas
Cytosolic LB1 (mCherry channel)
Nuclear membrane blebbing
CCF (DAPI channel)
f
Time (min) 0 15 30 45 105 120 135 330 345 390 495
GFP
mCherry
Merge
10 μm
g
mCherry-GFP-Lamin B1
DAPI
GFP
mCherry
LC3
Merge
Control
HRas V12
Inset
10 μm
20 μm
h
Control
HRasV12
% distribution of gold particles
Nuclear lamina
Nuclear plasma
Cytosol
Control HRasV12
Distribution of gold particles in HRasV12 cytosol
Autophagic vacuoles
Cytoplasm
Structures unidentified

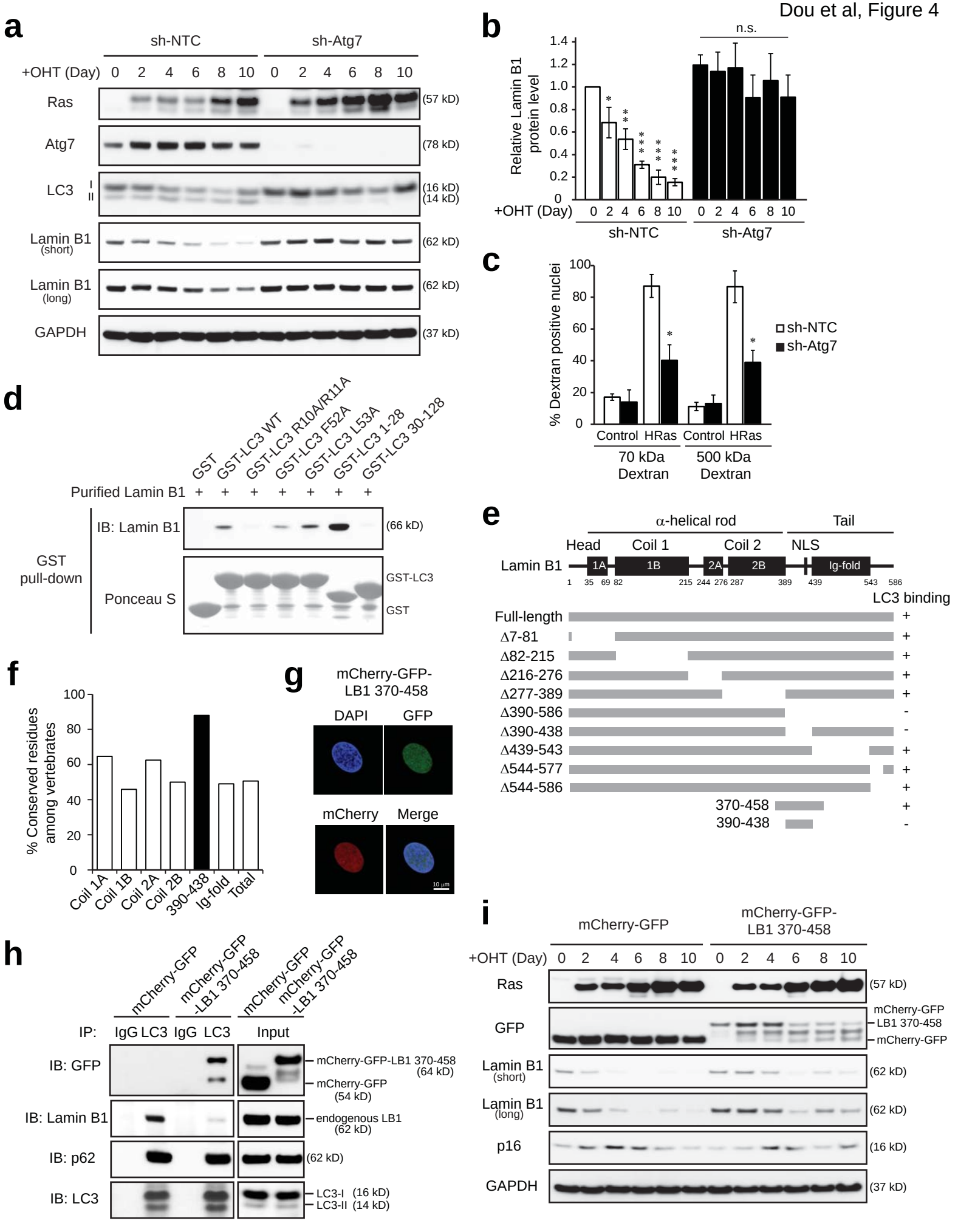
a
sh-NTC
sh-Atg7
+OHT (Day) 0 2 4 6 8 10 0 2 4 6 8 10
Ras
(57 kD)
Atg7
(78 kD)
LC3 I II
(16 kD)
(14 kD)
Lamin B1 (short)
(62 kD)
Lamin B1 (long)
(62 kD)
GAPDH
(37 kD)
b
n.s.
Relative Lamin B1 protein level
1.4
1.2
1.0
0.8
0.6
0.4
0.2
0
+OHT (Day) 0 2 4 6 8 10 0 2 4 6 8 10
sh-NTC
sh-Atg7
c
% Dextran positive nuclei
100
80
60
40
20
0
sh-NTC
sh-Atg7
Control HRas Control HRas
70 kDa Dextran
500 kDa Dextran
d
GST
GST-LC3 WT
GST-LC3 R10A/R11A
GST-LC3 F52A
GST-LC3 L53A
GST-LC3 1-28
GST-LC3 30-128
Purified Lamin B1 + + + + + + +
GST pull-down
IB: Lamin B1
(66 kD)
Ponceau S
GST-LC3
GST
e
α-helical rod
Tail
Head
Coil 1
Coil 2
NLS
Lamin B1
1A
1B
2A
2B
Ig-fold
1 35 69 82 215 244 276 287 389 439 543 586
LC3 binding
Full-length +
Δ7-81 +
Δ82-215 +
Δ216-276 +
Δ277-389 +
Δ390-586 -
Δ390-438 -
Δ439-543 +
Δ544-577 +
Δ544-586 +
370-458 +
390-438 -
f
% Conserved residues among vertebrates
100
80
60
40
20
0
Coil 1A
Coil 1B
Coil 2A
Coil 2B
390-438
Ig-fold
Total
g
mCherry-GFP-LB1 370-458
DAPI
GFP
mCherry
Merge
10 μm
h
mCherry-GFP
mCherry-GFP-LB1 370-458
mCherry-GFP
mCherry-GFP-LB1 370-458
IP: IgG LC3 IgG LC3 Input
IB: GFP
mCherry-GFP-LB1 370-458 (64 kD)
mCherry-GFP (54 kD)
IB: Lamin B1
endogenous LB1 (62 kD)
IB: p62
(62 kD)
IB: LC3
LC3-I (16 kD)
LC3-II (14 kD)
i
mCherry-GFP
mCherry-GFP-LB1 370-458
+OHT (Day) 0 2 4 6 8 10 0 2 4 6 8 10
Ras
(57 kD)
GFP
mCherry-GFP-LB1 370-458
mCherry-GFP
Lamin B1 (short)
(62 kD)
Lamin B1 (long)
(62 kD)
p16
(16 kD)
GAPDH
(37 kD)

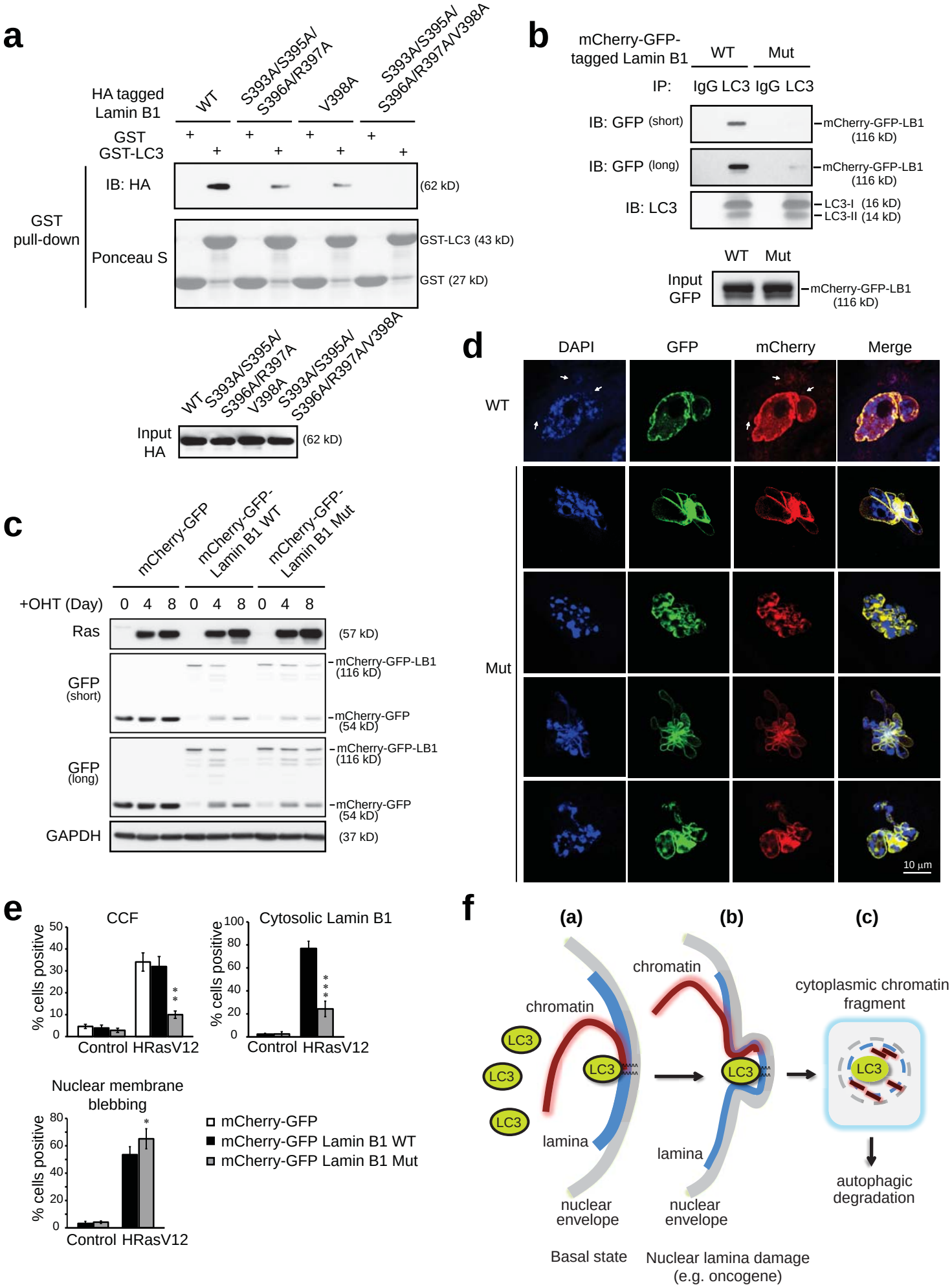
a
HA tagged Lamin B1
WT
S393A/S395A/ S396A/R397A
V398A
S393A/S395A/ S396A/R397A/V398A
GST
GST-LC3
IB: HA
(62 kD)
GST pull-down
Ponceau S
GST-LC3 (43 kD)
GST (27 kD)
Input HA
(62 kD)
b
mCherry-GFP-tagged Lamin B1
WT
Mut
IP:
IgG LC3 IgG LC3
IB: GFP (short)
IB: GFP (long)
IB: LC3
mCherry-GFP-LB1 (116 kD)
LC3-I (16 kD)
LC3-II (14 kD)
Input GFP
c
mCherry-GFP
mCherry-GFP-Lamin B1 WT
mCherry-GFP-Lamin B1 Mut
+OHT (Day)
0 4 8 0 4 8 0 4 8
Ras
(57 kD)
GFP (short)
GFP (long)
mCherry-GFP (54 kD)
GAPDH
(37 kD)
d
DAPI
GFP
mCherry
Merge
WT
Mut
10 μm
e
CCF
Cytosolic Lamin B1
% cells positive
Control HRasV12
Nuclear membrane blebbing
mCherry-GFP
mCherry-GFP Lamin B1 WT
mCherry-GFP Lamin B1 Mut
f
(a)
(b)
(c)
chromatin
LC3
lamina
nuclear envelope
cytoplasmic chromatin fragment
autophagic degradation
Basal state
Nuclear lamina damage (e.g. oncogene)